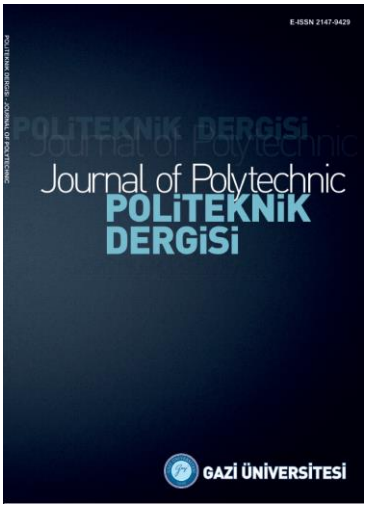

POLİTEKNİK DERGİSİ

JOURNAL of POLYTECHNIC

ISSN: 1302-0900 (PRINT), ISSN: 2147-9429 (ONLINE)
URL: http://dergipark.org.tr/politeknik

Investigation of compatibility between design and additively manufactured parts of functionally graded porous structures

İşlevsel geçişli gözenekli yapıların tasarımı ve eklemeli üretilen parçalar arasındaki uyumluluğun araştırılması

***Yazar(lar) (Author(s))**: Ahmet Murat DURSUN[1], Mehmet Çağrı TÜZEMEN[2], Elmas SALAMCİ[3], Oğuzhan YILMAZ[4], Rahmi ÜNAL[5],*

ORCID[1]: 0000-0001-9029-3246

ORCID[2]: 0000-0002-1746-2864

ORCID[3]: 0000-0003-2856-9402

ORCID[4]: 0000-0002-2641-2324

ORCID[5]: 0000-0001-5379-5159

Bu makaleye şu şekilde atıfta bulunabilirsiniz(To cite to this article): Dursun A. M., Tüzemen M. Ç., Salamci E., Yılmaz O. ve Ünal R., "Investigation of compatibility between design and additively manufactured parts of functionally graded porous structures", ***Politeknik Dergisi***, 25(3): 1069-1082, (2022).

Erişim linki (To link to this article): http://dergipark.org.tr/politeknik/archive

DOI: **10.2339/politeknik.891080**

Investigation of Compatibility Between Design and Additively Manufactured Parts of Functionally Graded Porous Structures

Highlights

- *Functionally graded porous structures were produced using the selective laser melting (SLM).*
- *Functionally graded porous structures were obtained by changing the unit cell size.*
- *Porosity measured by Archimedes and dry weighing method.*
- *Design and production differences were revealed with micro-computed tomography (micro-CT).*
- *Column thicknesses of specimens increased in the range of 150-300 μm compared to the design.*

Graphical Abstract

In this study, the design and production differences of functional graded porous structures produced by additive manufacturing were investigated. It was observed that the columns of the specimens became thicker compared to the design, sagging occurred on the horizontal columns and the porosity decreased.

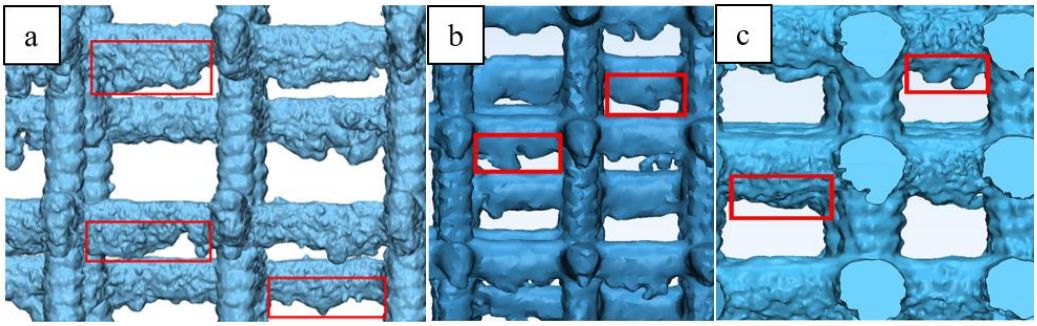

Figure. Molten material sagging on the horizontal columns of functionally graded porous structures

Aim

In this study, it is aimed to investigate the deviations for the porosity level of the Ti-6Al-4V functionally graded porous structures for three different cell structure types.

Design & Methodology

Nine different specimens were designed using three different unit cell structures and three different column thicknesses. Functionally graded porous structures were obtained by changing the unit cell size. Specimens produced by selective laser melting (SLM) and scanned by micro-CT. Porosity ratios were measured by Archimedes and dry weighing methods. After that the findings were compared with the design values.

Originality

Investigation of whether different unit cell structures and column thicknesses cause design and manufacturing differences in additive manufacturing.

Findings

An increase of 150-300 μm was observed on the column thicknesses of all functionally graded porous structures. Porosity of the manufactured parts was deviated by 5.71%-10.54% for cubic, 8.59%-12.39% for octahedroid, and 13%-16.49% for diamond compared to the design values.

Conclusion

It was concluded that the cell structure and column thickness do not influence the thickening of the column, but the cell structure influences the sagging of the columns. Porosity is affected by column thickening and sagging.

Declaration of Ethical Standards

The authors of this article declare that the materials and methods used in this study do not require ethical committee permission and/or legal-special permission.

Investigation of Compatibility Between Design and Additively Manufactured Parts of Functionally Graded Porous Structures

Araştırma Makalesi / Research Article

Ahmet Murat DURSUN[1], Mehmet Çağrı TÜZEMEN[2*], Elmas SALAMCİ[2], Oğuzhan YILMAZ[2], Rahmi ÜNAL[2]

[1]Medical Design and Production Center, University of Health Sciences, Ankara, Turkey
[2]Department of Mechanical Engineering, Gazi University, Ankara, Turkey

(Geliş/Received : 04.03.2021 ; Kabul/Accepted : 30.03.2021 ; Erken Görünüm/Early View : 21.04.2021)

ABSTRACT

In this study, deviations for the porosity level of the Ti-6Al-4V functionally graded porous structures for three different cell structures were investigated. For this purpose, functionally graded porous structures are designed and produced by selective laser melting (SLM). It is also aimed to investigate the effects of unit cell structure, unit cell size, and column (strut) thickness on the porosity deviation level. The specimens were scanned at micro-computed tomography (micro-CT) to determine the structure dimensions after production. According to the results obtained from micro-CT, an average increase of 150-300 μm was observed on the column thicknesses of all functionally graded porous structures. It has been observed that the horizontal columns of cubic and octagonal structures have sagging due to metal melting during production. It has been determined that the porosity of the manufactured parts was deviated between 5.71%-10.54% for cubic, 8.59%-12.39% for octahedroid, and 13%-16.49% for diamond structures compared to the design values.

Keywords: Additive manufacturing, porosity, functionally graded structure, micro-CT.

İşlevsel Geçişli Gözenekli Yapıların Tasarımı ve Eklemeli Üretilen Parçalar Arasındaki Uyumluluğun Araştırılması

ÖZ

Bu çalışmada, Ti-6Al-4V geçişli gözenekli yapıların üç farklı birim hücre yapısı için gözeneklilik oranlarındaki sapmalar araştırılmıştır. Bu amaçla, işlevsel geçişli hücresel yapılar tasarlanmış ve seçici lazer ergitme yöntemiyle üretilmiştir. Ayrıca birim hücre yapısının, birim hücre boyutunun ve kolon (dikme) kalınlığının gözenek boyutlarındaki sapma seviyesi üzerindeki etkilerinin araştırılması amaçlanmıştır. Numuneler, üretim sonrası yapı boyutunu belirlemek için mikro bilgisayarlı tomografide (mikro-BT) taranmıştır. Mikro-BT'den elde edilen sonuçlara göre, geçişli gözenekli tüm hücre yapılarının kolon kalınlık değerlerinde ortalama 150-300 μm arasında değişen artışlar gözlenmiştir. Kübik ve sekizyüzlü yapıların yatay kolonlarında üretim sırasında ergiyen metal sebebiyle sarkmalar oluştuğu gözlenmiştir. Üretilen parçaların gözenekliliği, tasarım değerleri ile karşılaştırıldığında kübik yapıda %5.71-%10.54, sekizyüzlü yapıda %8.59-12.39 ve elmas yapıda %13-16.49 aralıklarında değişen oranlarda sapmaların oluştuğu tespit edilmiştir.

Anahtar Kelimeler: Eklemeli üretim, gözeneklilik, işlevsel geçişli yapı, mikro-BT.

1. INTRODUCTION

There is an increased interest to produce open porous metallic lattice structures with regular unit cell architectures by additive manufacturing processes, which were impossible or difficult to manufacture using conventional techniques. Porous metal structures have the potential to provide lightweight and advanced or multifunctional properties. One of the production methods of porous structures is SLM. The gradually increased or decreased cell size can be applied by using this production method. Graded porous structures can provide superiority in terms of lightness, cost, and time for some applications such as medical implant and aerospace. There are several important parameters in the design of the graded porous structure. These can be listed as unit cell structure, unit cell size, and column thickness. These parameters significantly affect the porosity and the density of the structure. Among the design of the graded porous structure and the produced specimen, there are some geometric discrepancies mentioned in the literature, which result from the features of 3D printers using SLM technology. It is important to know these deviations for achieving the targeted structural values at the design stage.

**Sorumlu yazar (Corresponding Author)*
e-mail : cagrituzemen@gazi.edu.tr

Ti-6Al-4V is an important titanium alloy that combines strength and ductility. Therefore, Ti-6Al-4V alloy is frequently used in the production of porous structures [1–5]. Ti-6Al-4V alloy has excellent corrosion resistance due to the formation of an oxide layer on its surface. Also, it is preferred especially in medical implant applications because of its good biocompatibility and biomechanical properties [6–9]. The porous structures are used to improve thermal insulation properties, reduce weights, noise, and vibration in automotive and aerospace industries, meet mechanical properties close to bone tissue and assist in osseointegration of medical implants [10]. The necessity of maintaining open porosity is an advantage for applications such as bone replacement or filtration. Although this situation leads to reduction in theoretically achievable strength and stiffness. They are also used in the manufacture of composite parts and various filter applications [11].

Some researchers have stated that the minimum column thickness that can be produced by additive manufacturing technology is over 200-300 μm [12–14]. Mazur et al. were investigated the producibility of porous structures by SLM and a series of porous structures were produced from Ti-6Al-4V alloy material and it was stated that the minimum reproducible column thickness was 0.3 mm and the optimum unit cell size was 2-3 mm. They also stated that the porosity of the porous structures produced was higher in the range of 20-30% compared to the values obtained in the design, and that was due to additional structure formation and geometric deviations caused by the adherence of powder particles observed in the specimens [12]. Tsai et al. reported that column thickness of 400 μm showed the best biomechanical performance [15]. When choosing the column thickness, attention should be paid to the problems arising from the production variables of the 3D printer to be used. It is stated that the power of the laser, the diameter of laser focus, scanning speed, and scanning strategy used in the production cause the column thickness value to be higher in the production compared to the design [16–18]. These production parameters have been observed to cause expansion of the melt pool due to heat transfer between adjacent columns, and this expansion leads to increased column thickness as it increases powder adhesion on the columns [4, 17]. Due to the angles and dimensions of the structure elements, manufacturing defects can be observed in the production of different lattice structures [19, 20]. The increase in column thickness during production relative to the design value can cause in the closure of the open pores and consequently a reduction in the porosity of the lattice structure [17, 21]. Therefore, the column thickness should be kept under control. It has been determined that the high energy generated during the application of the laser on the powder causes splashes in the melt pool and these splashes disrupt the surface structure of the part and reduce the surface quality [22]. It has also been observed that this high energy creates heat diffusion between the columns and unit cells [17]. Heat diffusion causes the melt pool to grow, causing thickening of adjacent columns [16, 18, 23, 24]. The deviation values caused by these increases were found to be 150-200 μm [17, 23–25]. Since the geometric deviations caused by the production parameters cannot be predicted clearly, the open pores formed between the unit cells can cause contraction or even closure. Increases in column thickness and contraction in open pores cause a decrease in the porosity of porous structures. It has been reported that this decrease in the porosity reaches up to 23% [12, 26–28]. Bagheri et al. have been focused on the orientation angles of the columns to reduce dimensional mismatches between the design and production of porous structures made of Ti-6Al-4V alloy material by SLM. According to the study, a 60% deviation occurred due to high melting according to design values in horizontal columns to the production platform. They stated that dimensional deviation decreases as the angle of the columns goes from horizontal (0º) to vertical (90º). They emphasized that the reproducible column thickness value is over 200 μm [29].

In this study, it is aimed to investigate the deviations for the porosity level of graded porous structures have three unit cell structures. For this purpose, graded porous structures were designed and produced by SLM. It is also aimed to investigate the effects of unit cell structure, unit cell size, and column thickness on porosity deviation value. For this purpose, nine different design was created for the cubic, diamond, and octahedroid unit cell structure with using the same unit cell size and different column thicknesses. Design and experimental results were compared and discussed to determine the effects of cell structures on the deviation of porosity level.

2. MATERIAL AND METHOD

In this study, a total of nine graded porous structures with three different cell structures and three different column thicknesses for each cell structure were designed using the "3-Matic" software. This structure is a cylinder with a diameter of 21 mm and a length of 30 mm (Figure 1a). Diamond, cubic, and octahedroid were used as a unit cell structure. Three different structures were designed for each unit cell structure using column thicknesses of 0.3 mm, 0.5 mm, and 0.7 mm. Column thickness refers to the diameter of each rod in the unit cell. To form a graded porous structure, three different unit cell sizes were selected with increasing dimensions. Unit cell size refers to the length of an edge of the smallest unit cube to enclose each unit cell structure. Unit cell sizes were 1.8 mm, 2 mm, and 2.2 mm, respectively, from inside to outside (Figure 1b). Thus, variable porous structure with decreasing density from inside to outside was obtained. Dimensional selections in these designs were made to obtain values close to the porosity in human bones [3, 13, 15, 27, 30–32].The use of different unit cell sizes to form graded porous structures creates irregularities between transitions. These problems were solved by using auxiliary columns. For this study, a total of nine specimens were designed with three different unit cell

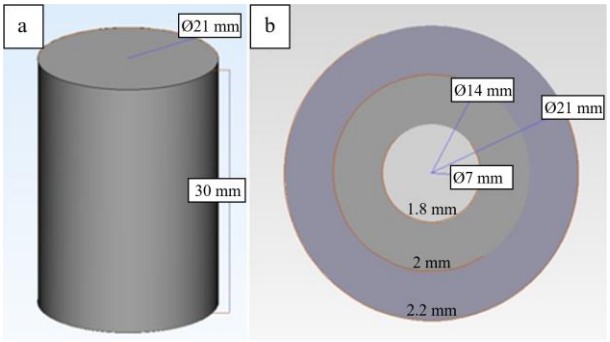

Figure 1. Specimen dimensions and cross-sectional view of the functionally graded porous structure. Dimensions within the region (1.8;2;2.2 mm) indicate the unit cell sizes in the relevant region

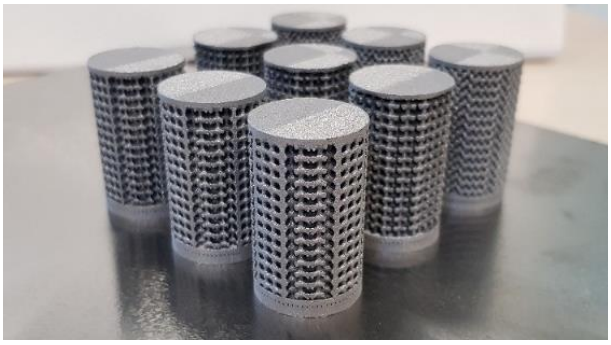

Figure 2. Post-production images of functionally graded porous structures

structures each of which has three different column thicknesses of 0.3 mm, 0.5 mm, and 0.7 mm.

To produce specimens by SLM, the support structure must be added. However, since the designed structures are porous, support cannot be added. To overcome this limitation, a shell has been added to the designs. The designed graded porous structures were sliced into 30 µm layers in the 3D printer's interface software (Magics RP), followed by the addition of supports. The designed graded porous structures were produced from Ti-6Al-4V (ELI grade 23) titanium alloy powder, as specified in ASTM F 136-02a [33]. SLM was used as an additive manufacturing technology. The production of functionally graded porous structures (Figure 2) was done by the Concept Laser M2 model 3D metal printer. Production parameters are given in Table 1. The production process was carried out under argon gas atmosphere. Graded porous structures were not treated with post-processes such as sandblasting or sanding. Only compressed air was sprayed to remove any residual powder and then held in an ultrasonic cleaner with purified water for 30 minutes.

Micro-computed tomography (micro-CT) and density measurement were applied to compare the compatibility of the produced graded porous structures with the design. Various geometric and morphological analyses can be performed by converting the data obtained from micro-CT to 3D form. Micro-CT has performed with Bruker Skyscan 1272 scanner at Hacettepe University Advanced Technologies Application and Research Center. The scans were performed at 100 kV voltage and 100 µA current. Specimens were scanned by rotating 360º with 0.6º scanning steps. Approximately 10 mm portions of the specimens were scanned vertically from the middle of the specimens. An average of 750 cross-sectional photographs were obtained for each specimen. The cross-sectional thickness of the scans for all samples is in the range of 15-21 µm. The obtained section images were reconstructed and corrected. The edited 2D section images were converted to 3D in Mimics software. Unit cell size and column thickness measurements were made from these images. Measurements and design data were compared.

For density measurement, porosity was calculated by using Archimedes [34–39] and dry weighing method, and deviations were determined by comparing with the porosity obtained in the design. Densities of the specimens were measured by Shimadzu SMK 401 in the Powder Metallurgy Laboratory of Gazi University. For Archimedes measurements, samples were first weighed in air (Figure 3a) and then in water (Figure 3b). The water temperature during weighing was measured at 14°C. Since the density of the water depends on the temperature, the temperature during the measurements is important. Each of the specimens was covered with plastic film to prevent water from entering the open pores. The weight of each film-covered sample was measured on the density kit of the device, first in the air and then in water. The air weight of the films was subtracted from the air weight of each film-covered specimen and the net weight of the specimen was measured. After calculating the weights and densities of the specimens, it was aimed to calculate the porosity in

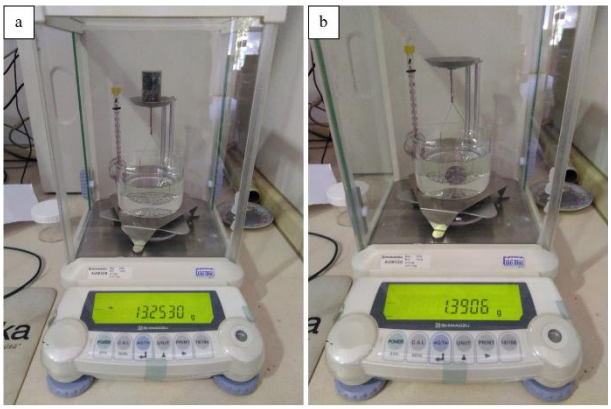

Figure 3. Weighing the specimens in air (a) and water (b)

Table 1. Production parameters

Ti-6Al-4V powder shape and diameter	Density of powder	Production layer thickness	Laser power (Max.)	Laser scanning speed (Max.)	Diameter of laser focus
Spherical 10-45µm	4.43 gr/cm^3	30 µm	200 W	1800 mm/s	150 µm

the structures and these experimental data were compared with the values obtained from the design.

3. RESULT AND DISCUSSION

3.1. Micro-Computed Tomography Findings

Produced nine graded porous structures were scanned by micro-CT and the results were examined separately according to unit cell structures.

3.1.1. Cubic structures

A micro-CT image of a 0.3 mm column thickness specimen with a cubic unit cell structure was given in Figure 4. The area between green and blue was defined as layer 1 transition, the area between blue and red was defined as layer 2 transition, and the area within red was defined as layer 3 transition. Figure 4 shows the unit cell size, column thickness, and pore size values of the graded porous lattice structure. Design measures; unit cell size (a) 2.2; 2; 1.8 mm (from outside to inside, respectively), pore size 1.9; 1.7; 1.5 mm (from outside to inside, respectively) and column thickness (d) 0.3 mm.

In Figure 5 and Figure 6, micro-CT images of the specimens having column thicknesses of 0.5 mm and 0.7 mm are given, respectively. When the cross-sectional images of the graded porous cubic porous structures were examined, column thickness increases were observed up to 200 μm. These increases were observed to occur independently of the unit cell size. No significant change in unit cell size was noticed. Due to the increase in column thickness, pore sizes within the unit cells were decreased by the amount of increase in column thickness, or very close.

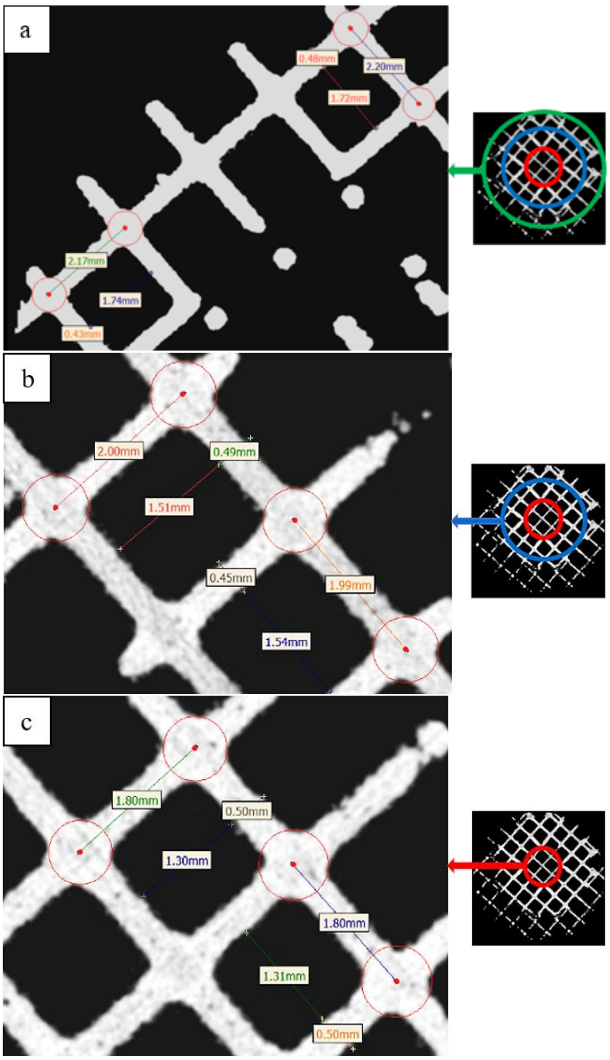

Figure 4. Micro-CT images of the graded porous cubic structure (d=0.3 mm) 1st layer transition (a=2.2 mm) (a), 2nd layer transition (a=2 mm) (b), 3rd layer transition (a=1.8 mm) (c)

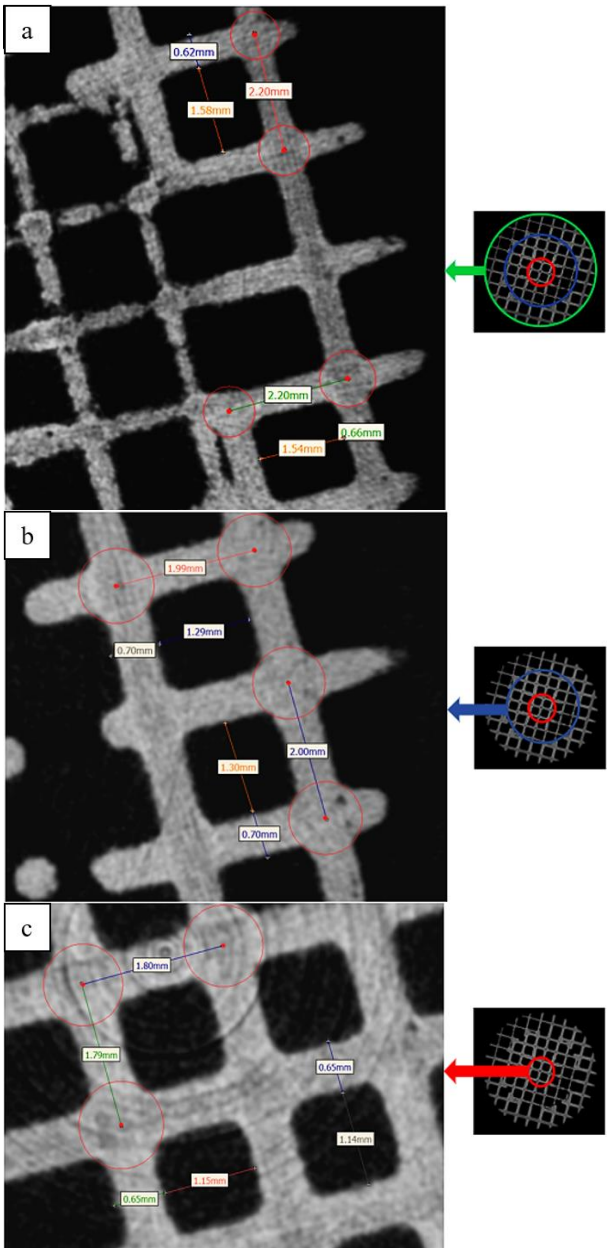

Figure 5. Micro-CT images of the graded porous cubic structure (d=0.5 mm) 1st layer transition (a=2.2 mm) (a), 2nd layer transition (a=2 mm) (b), 3rd layer transition (a=1.8 mm) (c)

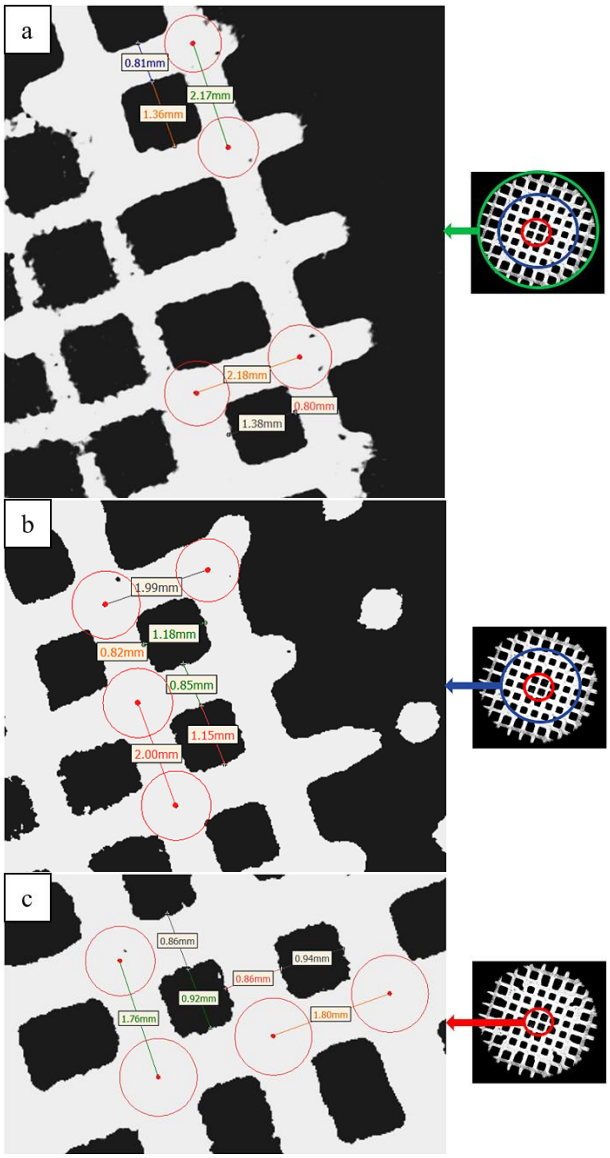

Figure 6. Micro-CT images of the graded porous cubic structure (d=0.7 mm) 1st layer transition (a=2.2 mm) (a), 2nd layer transition (a=2 mm) (b), 3rd layer transition (a=1.8 mm) (c)

3.1.2. Octahedroid structures

A micro-CT image of the specimen with a column thickness of 0.3 mm from the specimens produced using the octahedroid unit cell structure is given in Figure 7. The area between green and blue is defined as layer 1 transition, the area between blue and red is defined as layer 2 transition, and the area within red is defined as layer 3 transition. Figure 7 shows the unit cell size, column thickness, and pore size values of the graded porous lattice structure. Design measures; unit cell size (a) 2.2; 2; 1.8 mm (from outside to inside, respectively), pore size 1.9; 1.7; 1.5 mm (from outside to inside, respectively) and column thickness (d) 0.3 mm. In Figure 8 and Figure 9, micro-CT images of the specimens having column thicknesses of 0.5 mm and 0.7 mm are given, respectively. When the cross-sectional images of the graded porous octahedroid porous structures were

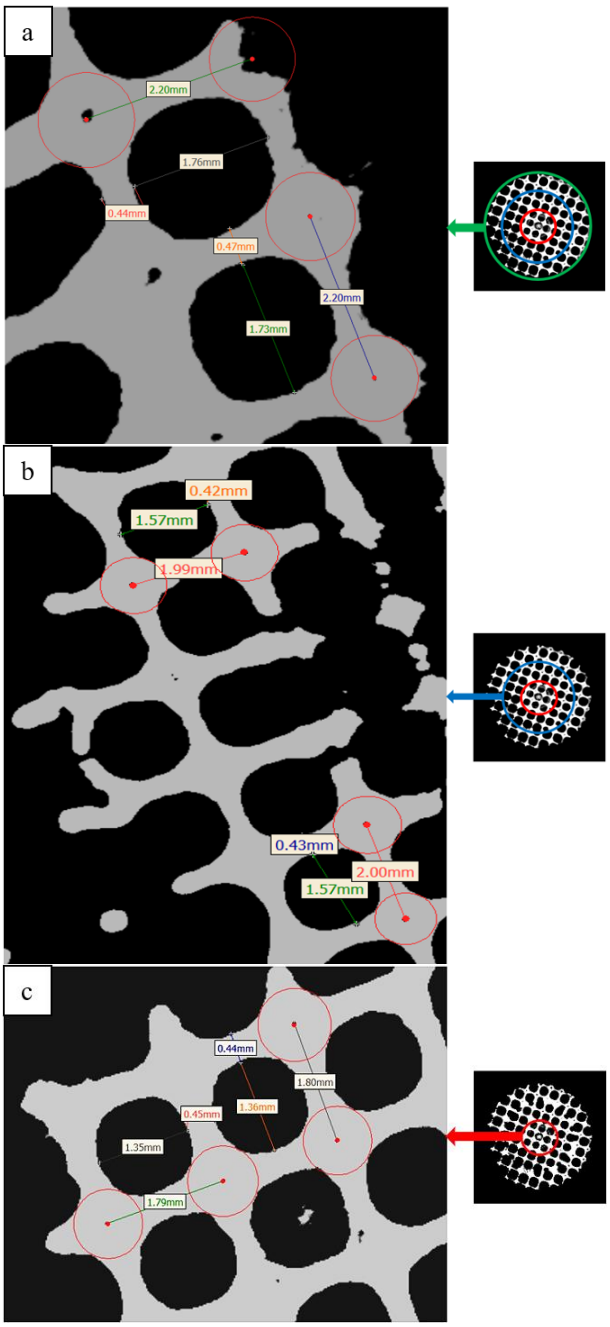

Figure 7. Micro-CT images of the graded porous octahedroid structure (d=0.3 mm) 1st layer transition (a=2.2 mm) (a), 2nd layer transition (a=2 mm) (b), 3rd layer transition (a=1.8 mm) (c)

examined, column thickness increases were observed up to 200 µm, like the cubic structure.

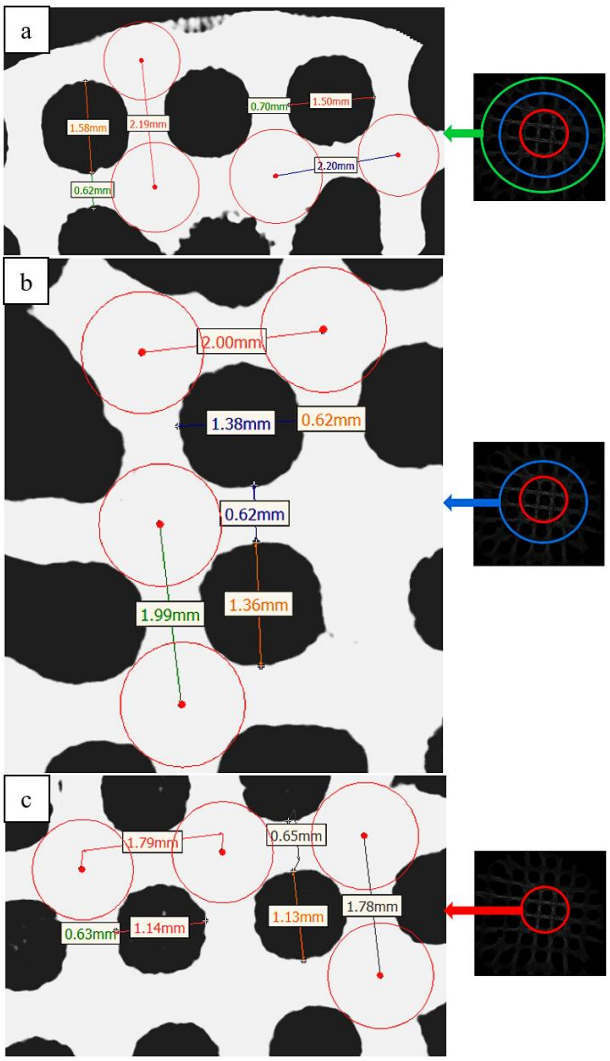

Figure 8. Micro-CT images of the graded porous octahedroid structure (d=0.5 mm) 1st layer transition (a=2.2 mm) (a), 2nd layer transition (a=2 mm) (b), 3rd layer transition (a=1.8 mm) (c)

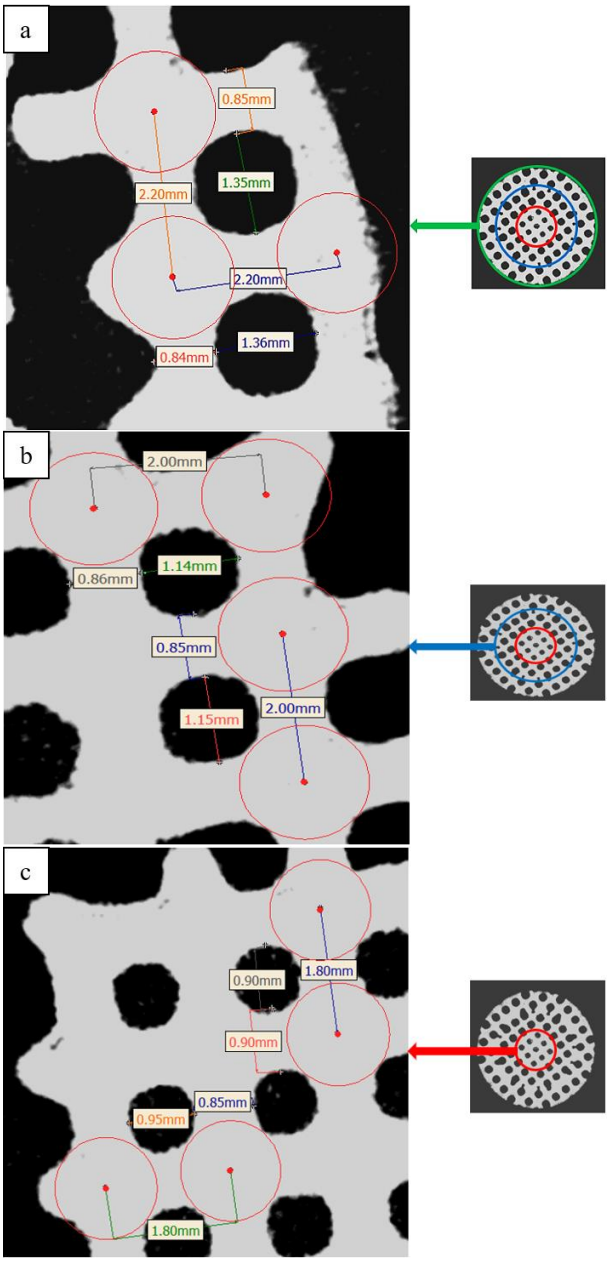

Figure 9. Micro-CT images of the graded porous octahedroid structure (d=0.7 mm) 1st layer transition (a=2.2 mm) (a), 2nd layer transition (a=2 mm) (b), 3rd layer transition (a=1.8 mm) (c)

3.1.3. Diamond structures

A micro-CT image of the specimen with a column thickness of 0.3 mm from the specimens produced using the diamond unit cell structure is given in Figure 10. The area between green and blue is defined as layer 1 transition, the area between blue and red is defined as layer 2 transition, and the area within red is defined as layer 3 transition. Figure 10 shows the unit cell size, column thickness, and pore size values of the graded porous lattice structure. Design measures; unit cell size (a) 2.2; 2; 1.8 mm (from outside to inside, respectively), pore size 1.9; 1.7; 1.5 mm (from outside to inside, respectively) and column thickness (d) 0.3 mm. In Figure 11 and Figure 12, micro-CT images of the specimens having column thicknesses of 0.5 mm and 0.7 mm are given, respectively. When the cross-sectional images of the graded porous diamond porous structures were examined, column thickness increases were observed up to 300 µm.

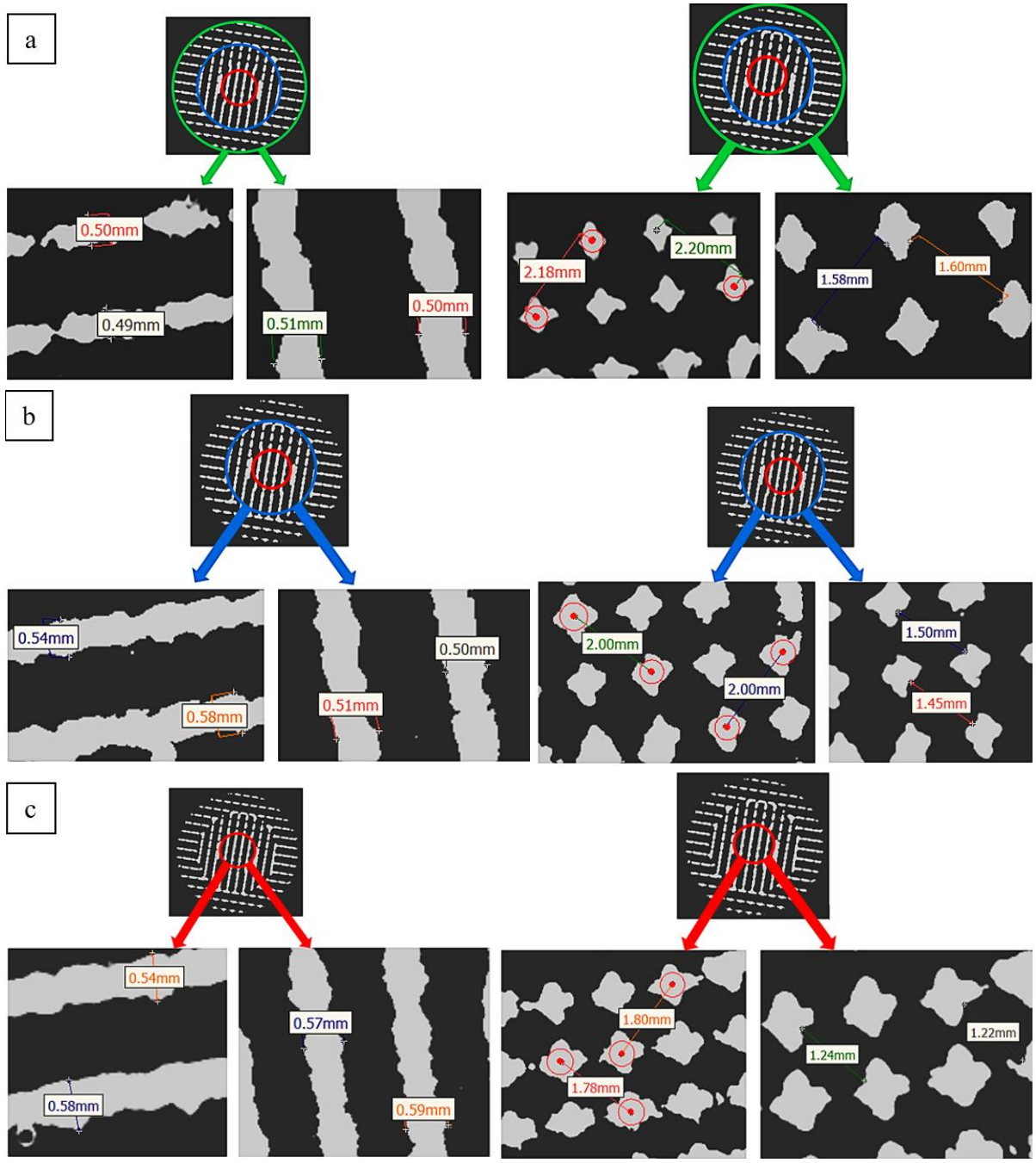

Figure 10. Micro-CT images of the graded porous diamond structure (d=0.3 mm) 1st layer transition (a=2.2 mm) (a), 2nd layer transition (a=2 mm) (b), 3rd layer transition (a=1.8 mm) (c)

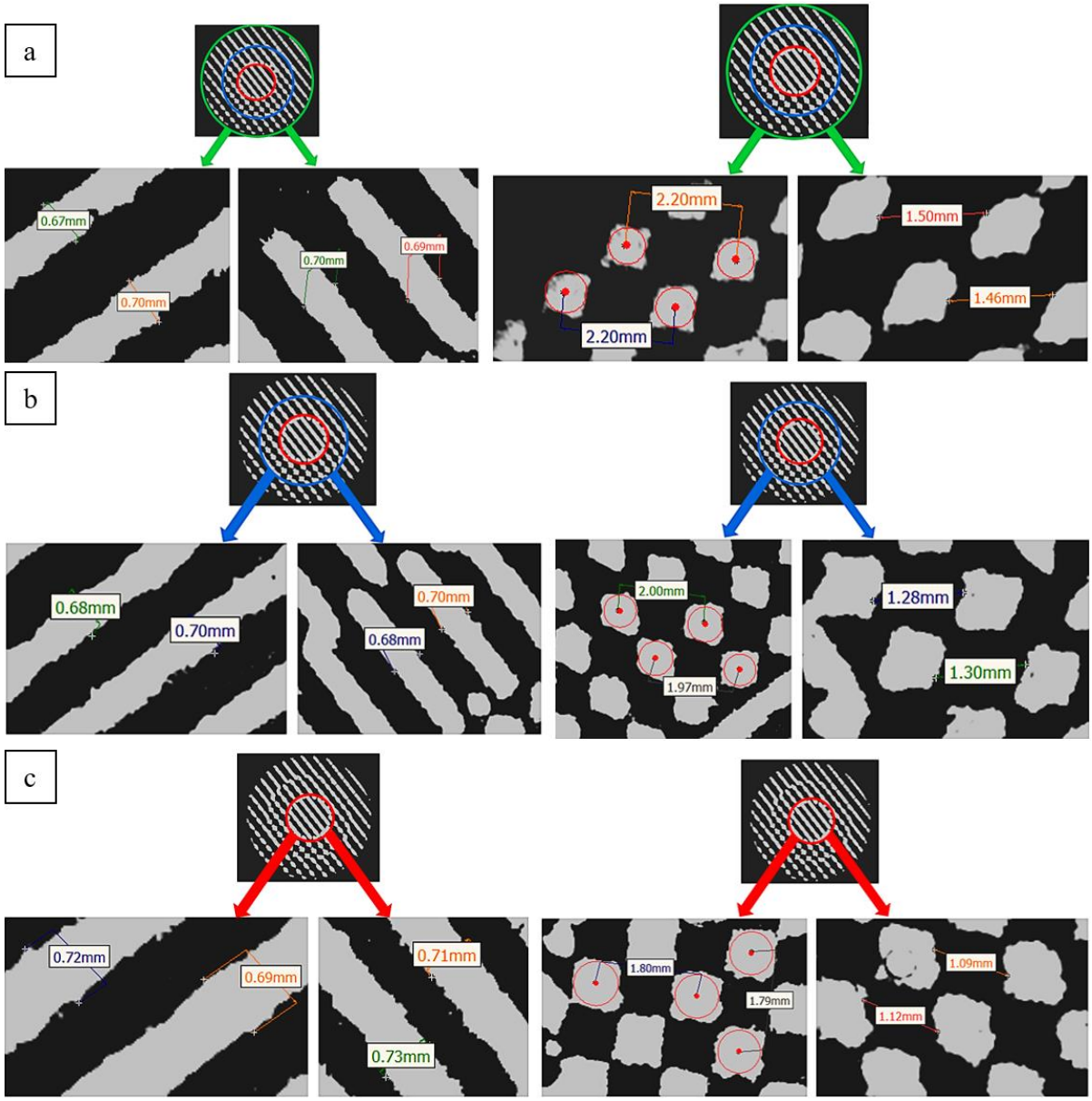

Figure 11. Micro-CT images of the graded porous diamond structure (d=0.5 mm) 1st layer transition (a=2.2 mm) (a), 2nd layer transition (a=2 mm) (b), 3rd layer transition (a=1.8 mm) (c)

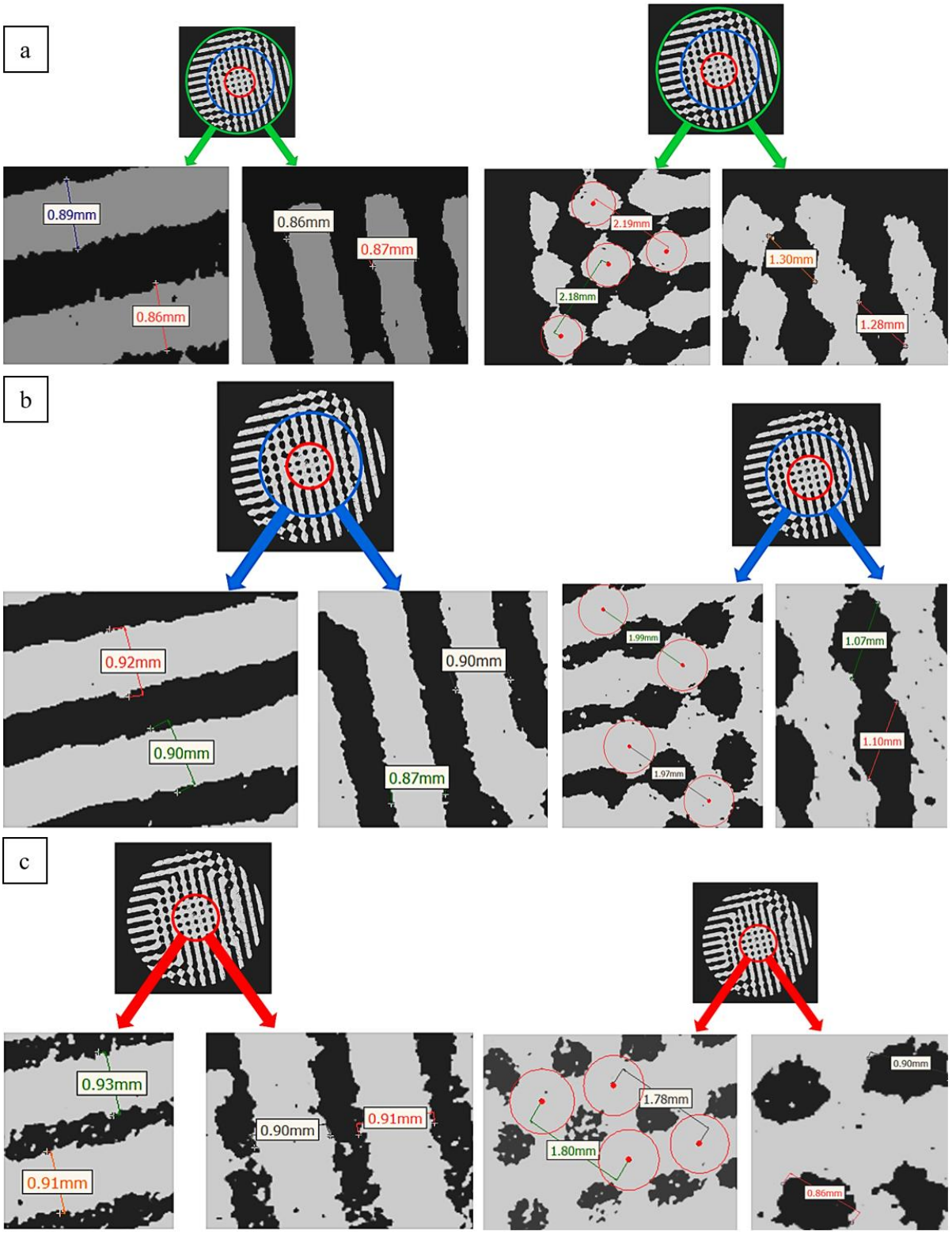

Figure 12. Micro-CT images of the graded porous diamond structure (d=0.7 mm) 1st layer transition (a=2.2 mm) (a), 2nd layer transition (a=2 mm) (b), 3rd layer transition (a=1.8 mm) (c)

2D scanning images obtained from the Micro-CT were converted to 3D. It was determined that the sagging of the molten material occurred due to the dispersion of the molten metal in places parallel to the production platform of the structure which could not be supported (Figure 13). Increases of column thicknesses up to 650 µm, 500 µm and 500 µm were observed in the specimens having 0.3 mm, 0.5 mm and 0.7 mm column thicknesses respectively on the horizontal axis of the sagging areas. In octahedroid structures, just as in cubic structures, the sagging occurred due to the dispersion of the molten metal on columns parallel to the production base of the structure which could not be supported (Figure 14). Increases of column thicknesses up to 500 µm, 450 µm, and 550 µm were observed in the specimens having 0.3 mm, 0.5 mm, and 0.7 mm column thicknesses respectively on the horizontal axis of the sagging areas. In diamond structures, the sagging of the molten material caused by the dispersion of the molten metal is much less compared to cubic and octahedroid unit cell structures (Figure 15). These reductions are thought to occur because the columns of the diamond unit cell structure are positioned at an angle to the production platform.

According to the results of micro-CT, dimensional values obtained in production were always larger than dimensional values in design. To increase the controllability of the parts with high precision, it is necessary to make changes in the production parameters.

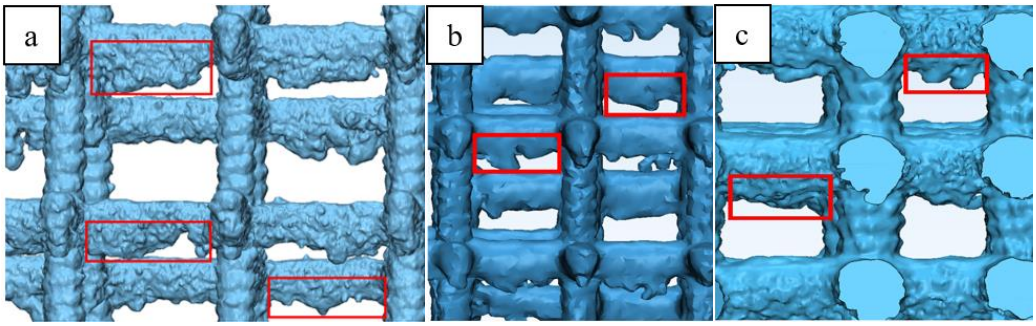

Figure 13. Molten material sagging on the horizontal axis of (a) 0.3 mm (b) 0.5 mm and (c) 0.7 mm column thickness samples with the graded porous cubic porous structure

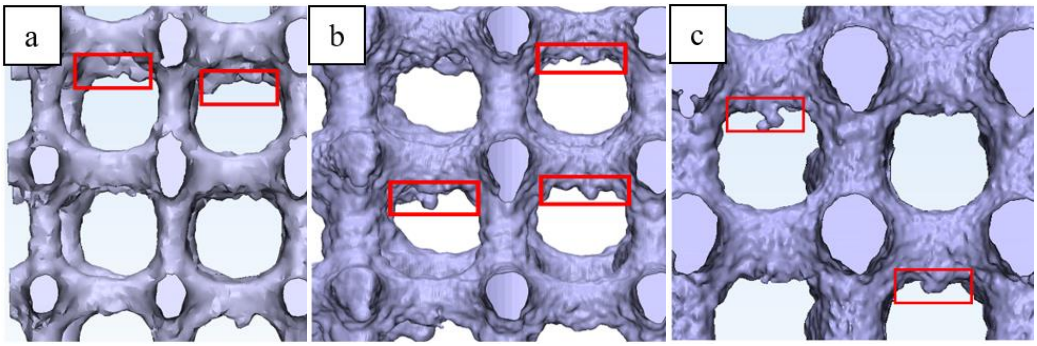

Figure 14. Molten material sagging on the horizontal axis of (a) 0.3 mm (b) 0.5 mm and (c) 0.7 mm column thickness samples with graded porous octahedroid porous structure

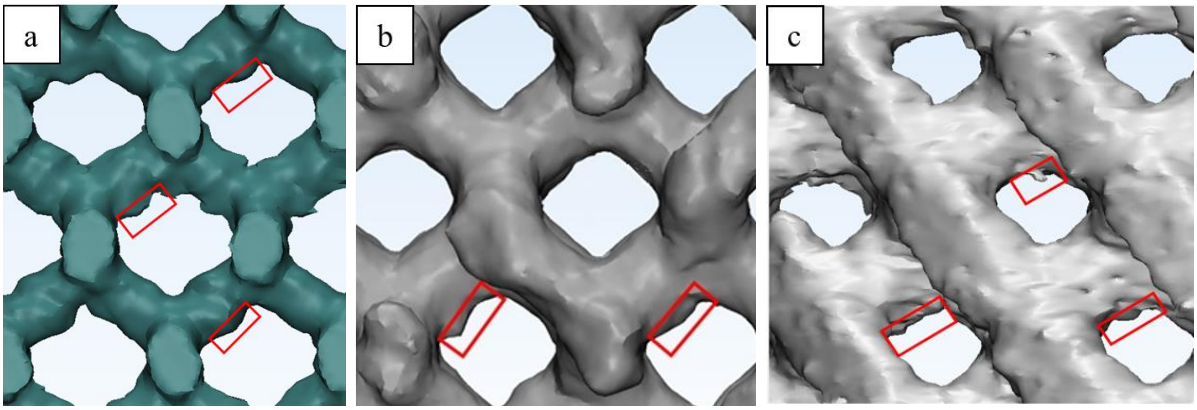

Figure 15. Molten material sagging on the horizontal axis of (a) 0.3 mm (b) 0.5 mm and (c) 0.7 mm column thickness samples with the graded porous diamond porous structure

The reason for these differences between the design and production of column thicknesses is the production parameters (laser power, scanning speed, scanning strategy, etc.) of the 3D metal printer. Factors such as powder adhesion and spattering reduce dimensional accuracy [16, 18, 27, 40, 41]. Dimensional expansion of column thickness of all graded porous structures occurred in the range of 150-300 µm compared to the design. Decreases in pore sizes of porous structures with increasing column thickness were observed as much as the amount of increase in column thickness. It has been found that these increases occur independently of the unit cell size, which also means that the increase in the column thickness is independent of being graded. Molten material sagging up to 550 µm was observed in the thickness of the columns parallel to the production platform of cubic and octahedroid porous structures. In the diamond graded porous structure, no significant increase was observed in the sagging of the molten material due to the columns being closer to perpendicular to the production platform.

Functionally graded porous structures porosities were calculated by using the Archimedes method. Also, the porosities were calculated by weighing the specimens dry on the density kit and all data were compared with the porosities obtained from the designs of the samples. The porosities of the functionally graded porous structures

Table 2. Comparison of porosities and percentage error of functionally graded porous structures

		Porosity (%)			Deviation (%)	
Specimen	Column thickness [mm]	Design	Archimedes	Dry weighing	Design-Archimedes	Design-Dry weighting
Diamond	0.3	84.26	73.30	73.73	13	12.49
Diamond	0.5	69.48	59.09	59.48	14.95	14.39
Diamond	0.7	51.72	43.19	43.30	16.49	16.27
Cubic	0.3	89.54	84.42	84.31	5.71	5.84
Cubic	0.5	82.62	74.09	76.32	10.32	7.62
Cubic	0.7	73.60	65.84	67.21	10.54	8.68
Octahedroid	0.3	84.84	77.55	77.91	8.59	8.16
Octahedroid	0.5	75.58	66.21	68.89	12.39	8.85
Octahedroid	0.7	65.91	58.46	59.30	11.30	10.02

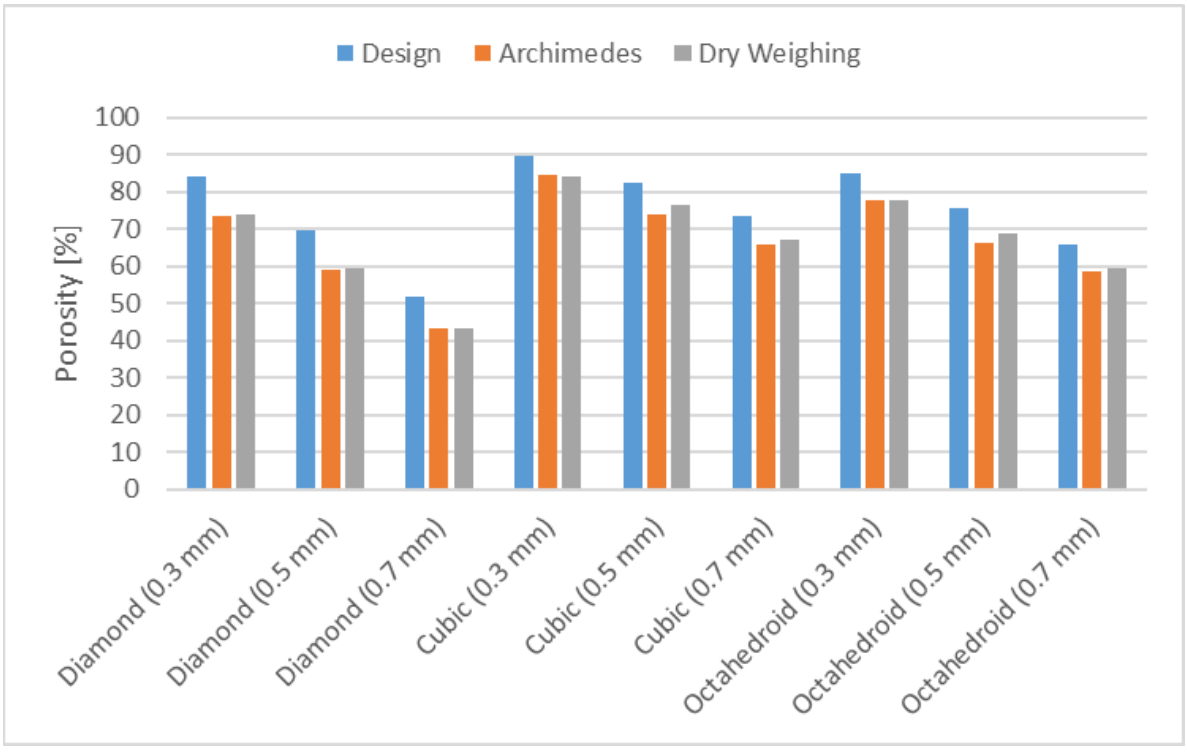

Figure 16. Porosity ratios of functionally graded porous structures. Dimensions in parentheses indicate the column thickness

and the differences between measurement and design are given in Table 2. The results are presented graphically in Figure 16.

It has been determined that the porosity (Archimedes) of the specimens was decreased by 5.71%-10.54% for cubic, 8.59%-12.39% for octahedroid, and 13%-16.49% for diamond compared to the design values. Porosities obtained by Archimedes and dry weighing methods are close to each other. According to the porosities obtained from the design data, the lower porosities in Archimedes and dry weighing methods were caused by the increase in column thickness because of molten material sagging. The lower porosities in Archimedes and dry weighing methods compared to the design were due to the column thickness increases described in the micro-CT results. It has been observed that 1 mm shells, which are used to hold the support material, cause more than a 6% reduction in the porosities of the structures. The auxiliary columns formed to allow the adherence of the graded porous structures to each other in layer transitions are effective in decreasing the porosities. Increases in column thickness resulted in deviations of less than 2% resulting in increases in specimen's length and diameter of about 200 μm. The porosity deviation rates increase as column thickness increases in most specimens. Since there are more columns in the diamond unit cell structure, the porosity of diamond is less than the other structures for the same column thicknesses.

4. CONCLUSION

In this study, functionally graded porous structures were produced by SLM method using Ti-6Al-4V. A total of nine different specimens were produced using three different unit cell structures (diamond, cubic, and octahedroid) and three different column thicknesses (0.3, 0.5, and 0.7 mm) for each cell structure. The differences between design and production were investigated using micro-CT, Archimedes and dry weighing methods. Micro-CT results reveal the increase in column thickness of the porous structures due to the sagging of the molten material. The average increase in column thickness was 200 μm. This increase depended on the angle between the columns and the production platform. However, these increases occurred regardless of column thickness and unit cell structure. The increase in column thickness caused a decrease in porosity. The decrease in the porosities of the structures was determined by the application of Archimedes and dry weighing method. According to the results of the Archimedes method, the porosities of the graded porous structures were decreased by 5.71-10.54% for cubic, 8.59-12.39% for octahedroid, and 13-16.49% for diamond compared to design values. In future studies, variables such as laser focus diameter, laser power, and scanning strategy can be studied parametrically and the effect of each can be examined separately in order to control these increases and eliminate the differences between design and production.

ACKNOWLEDGEMENT

This work was supported by the Scientific and Technological Research Council of Turkey (TÜBİTAK) [Grant number MAG-116R021].

DECLARATION OF ETHICAL STANDARDS

The authors of this article declare that the materials and methods used in this study do not require ethical committee permission and/or legal-special permission.

AUTHORS' CONTRIBUTIONS

Ahmet Murat DURSUN: Conceptualization, performed the experiments and analyse the results.

Mehmet Çağrı TÜZEMEN: Conceptualization, analyse the results and wrote the manuscript.

Elmas SALAMCİ: Review the manuscript.

Oğuzhan YILMAZ: Review the manuscript.

Rahmi ÜNAL: Conceptualization, review the manuscript, supervision and project administration.

CONFLICT OF INTEREST

There is no conflict of interest in this study.

REFERENCES

[1] Zhang X. Y., Fang G., Leeflang S., Zadpoor A. A., and Zhou J., "Topological design, permeability and mechanical behavior of additively manufactured functionally graded porous metallic biomaterials", **Acta Biomaterialia**, 84: 437–452, (2019).

[2] Zhang X. Y., Yan X. C., Fang G., and Liu M., "Biomechanical influence of structural variation strategies on functionally graded scaffolds constructed with triply periodic minimal surface", **Additive Manufacturing**, 32: 101015, (2020).

[3] Zhao D., Huang Y., Ao Y., Han C., Wang Q., Li Y., Liu J., Wei Q., and Zhang Z., "Effect of pore geometry on the fatigue properties and cell affinity of porous titanium scaffolds fabricated by selective laser melting", **Journal of the Mechanical Behavior of Biomedical Materials**, 88: 478–487, (2018).

[4] Dallago M., Fontanari V., Winiarski B., Zanini F., Carmignato S., and Benedetti M., "Fatigue properties of Ti6Al4V cellular specimens fabricated via SLM: CAD vs real geometry", **Procedia Structural Integrity**, 7: 116–123, (2017).

[5] Ali H., Ghadbeigi H., and Mumtaz K., "Processing Parameter Effects on Residual Stress and Mechanical Properties of Selective Laser Melted Ti6Al4V", **Journal of Materials Engineering and Performance**, 27: 4059–4068, (2018).

[6] Aydın İ., and Engin F., "Hydroxyapatite Coating on Ti6Al4V Alloy Surface Through Biomimetic Method Using Glycolic Acid - Sodium Gluconate Buffer System and Examination of Properties of the Coating", **Journal of Polytechnic**, 20: 993–1001, (2017).

[7] Subaşi M., Safarian A., and Karataş Ç., "An Investigation of Sintering Parameters of Ti-6Al-7Nb Fabricated by Powder Injection Molding", **Journal of Polytechnic**, 30: 502–512, (2017).

[8] Subasi O., Oral A., and Lazoglu I., "A novel adjustable locking plate (ALP) for segmental bone fracture treatment", **Injury**, 50: 1612–1619, (2019).

[9] Wu L., and Zhang J., "Phase Field Simulation of Dendritic Solidification of Ti-6Al-4V During Additive Manufacturing Process", **Jom**, 70: 2392–2399, (2018).

[10] Challis V. J., Xu X., Zhang L. C., Roberts A. P., Grotowski J. F., and Sercombe T. B., "High specific strength and stiffness structures produced using selective laser melting", **Materials and Design**, 63: 783–788, (2014).

[11] Gibson L. J., and Ashby M. F., Cellular solids: Structure and properties, second edition. Cell Solids Struct Prop Second Ed.

[12] Mazur M., Leary M., McMillan M., Sun S., Shidid D., and Brandt M., "Mechanical properties of Ti6Al4V and AlSi12Mg lattice structures manufactured by Selective Laser Melting (SLM)", **Laser Additive Manufacturing: Materials, Design, Technologies, and Applications**, 119–161, (2017).

[13] Arabnejad S., Burnett Johnston R., Pura J. A., Singh B., Tanzer M., and Pasini D., "High-strength porous biomaterials for bone replacement: A strategy to assess the interplay between cell morphology, mechanical properties, bone ingrowth and manufacturing constraints", **Acta Biomaterialia**, 30: 345–356, (2016).

[14] Zhang S., Wei Q., Cheng L., Li S., and Shi Y., "Effects of scan line spacing on pore characteristics and mechanical properties of porous Ti6Al4V implants fabricated by selective laser melting", **Materials and Design**, 63: 185–193, (2014).

[15] Tsai P. I., Hsu C. C., Chen S. Y., Wu T. H., and Huang C. C., "Biomechanical investigation into the structural design of porous additive manufactured cages using numerical and experimental approaches", **Computers in Biology and Medicine**, 76: 14–23, (2016).

[16] Sing S. L., Yeong W. Y., Wiria F. E., and Tay B. Y., "Characterization of Titanium Lattice Structures Fabricated by Selective Laser Melting Using an Adapted Compressive Test Method", **Experimental Mechanics**, 56: 735–748, (2016).

[17] Van Bael S., Kerckhofs G., Moesen M., Pyka G., Schrooten J., and Kruth J. P., "Micro-CT-based improvement of geometrical and mechanical controllability of selective laser melted Ti6Al4V porous structures", **Materials Science and Engineering A**, 528: 7423–7431, (2011).

[18] Xu Y., Zhang D., Zhou Y., Wang W., and Cao X., "Study on topology optimization design, manufacturability, and performance evaluation of Ti-6Al-4V porous structures fabricated by selective laser melting (SLM)", **Materials**, 10 (9): 1048, (2017).

[19] Balcı A., Küçükaltun F., Aycan M. F., Usta Y., and Demir T., "Reproducibility of Replicated Trabecular Bone Structures from Ti6Al4V Extralow Interstitials Powder by Selective Laser Melting", **Arabian Journal for Science and Engineering**, 46: 2527–2541, (2021).

[20] Balcı A., Aycan M. F., Usta Y., and Demir T., "Seçimli Lazer Ergitme İle Ti6Al4V ELI Alaşımından Üretilen Trabeküler Metal Yapıların Basma Ve Basma-Kayma Dayanımlarının İncelenmesi", **Journal of Polytechnic**, 1–1, (2020).

[21] Mullen L., Stamp R. C., Brooks W. K., Jones E., and Sutcliffe C. J., "Selective laser melting: A regular unit cell approach for the manufacture of porous, titanium, bone in-growth constructs, suitable for orthopedic applications", **Journal of Biomedical Materials Research - Part B Applied Biomaterials**, 89: 325–334, (2009).

[22] Bai Y., Wang D., Yang Y., and Wang H., "Effect of heat treatment on the microstructure and mechanical properties of maraging steel by selective laser melting", **Materials Science and Engineering A**, 760: 105–117, (2019).

[23] Li S. J., Xu Q. S., Wang Z., Hou W. T., Hao Y. L., Yang R., and Murr L. E., "Influence of cell shape on mechanical properties of Ti-6Al-4V meshes fabricated by electron beam melting method", **Acta Biomaterialia**, 10: 4537–4547, (2014).

[24] Van Bael S., Chai Y. C., Truscello S., Moesen M., Kerckhofs G., Van Oosterwyck H., Kruth J. P., and Schrooten J., "The effect of pore geometry on the in vitro biological behavior of human periosteum-derived cells seeded on selective laser-melted Ti6Al4V bone scaffolds", **Acta Biomaterialia**, 8: 2824–2834, (2012).

[25] Warnke P. H., Douglas T., Wollny P., Sherry E., Steiner M., Galonska S., Becker S. T., Springer I. N., Wiltfang J., and Sivananthan S., "Rapid prototyping: Porous titanium alloy scaffolds produced by selective laser melting for bone tissue engineering", **Tissue Engineering - Part C: Methods**, 15: 115–124, (2009).

[26] Han C., Li Y., Wang Q., Wen S., Wei Q., Yan C., Hao L., Liu J., and Shi Y., "Continuous functionally graded porous titanium scaffolds manufactured by selective laser melting for bone implants", **Journal of the Mechanical Behavior of Biomedical Materials**, 80: 119–127, (2018).

[27] Emmelmann C., Scheinemann P., Munsch M., and Seyda V., "Laser additive manufacturing of modified implant surfaces with osseointegrative characteristics", **Physics Procedia**, 12: 375–384, (2011).

[28] Parthasarathy J., Starly B., Raman S., and Christensen A., "Mechanical evaluation of porous titanium (Ti6Al4V) structures with electron beam melting (EBM)", **Journal of the Mechanical Behavior of Biomedical Materials**, 3: 249–259, (2010).

[29] Bagheri Z. S., Melancon D., Liu L., Johnston R. B., and Pasini D., "Compensation strategy to reduce geometry and mechanics mismatches in porous biomaterials built with Selective Laser Melting", **Journal of the Mechanical Behavior of Biomedical Materials**, 70: 17–27, (2017).

[30] Weißmann V., Wieding J., Hansmann H., Laufer N., Wolf A., and Bader R., "Specific yielding of selective laser-melted Ti6Al4V open-porous scaffolds as a function of unit cell design and dimensions", **Metals**, 6 (7): 166, (2016).

[31] Nune K. C., Kumar A., Misra R. D. K., Li S. J., Hao Y. L., and Yang R., "Osteoblast functions in functionally

graded Ti-6Al-4 v mesh structures", **Journal of Biomaterials Applications**, 30: 1182–1204, (2016).

[32] Shi J., Yang J., Li Z., Zhu L., Li L., and Wang X., "Design and fabrication of graduated porous Ti-based alloy implants for biomedical applications", **Journal of Alloys and Compounds**, 728: 1043–1048, (2017).

[33] ASTM F 136-02A, "Standard specification for wrought titanium-6aluminum-4vanadium eli (extra low interstitial) alloy for surgical implant applications", (2002) .

[34] Spierings A. B., Schneider M., and Eggenberger R., "Comparison of density measurement techniques for additive manufactured metallic parts", **Rapid Prototyping Journal**, 17: 380–386, (2011).

[35] Romano S., Abel A., Gumpinger J., Brandão A. D., and Beretta S., "Quality control of AlSi10Mg produced by SLM: Metallography versus CT scans for critical defect size assessment", **Additive Manufacturing**, 28: 394–405, (2019).

[36] Pyka G., Kerckhofs G., Schrooten J., and Wevers M., "The effect of spatial micro-CT image resolution and surface complexity on the morphological 3D analysis of open porous structures", **Materials Characterization**, 87: 104–115, (2014).

[37] Gong H., Nadimpalli V. K., Rafi K., Starr T., and Stucker B., "Micro-CT Evaluation of Defects in Ti-6Al-4V Parts Fabricated by Metal Additive Manufacturing", **Technologies**, 7: 44, (2019).

[38] Zhou X., Dai N., Chu M., Wang L., Li D., Zhou L., and Cheng X., "X-ray CT analysis of the influence of process on defect in Ti-6Al-4V parts produced with Selective Laser Melting technology", **The International Journal of Advanced Manufacturing Technology**, 106 (1): 3-14, (2020).

[39] Liu Y., Li X., Chen C., Song Y., and Ni P., "High throughput rapid detection for SLM manufactured elements using ultrasonic measurement", **Measurement: Journal of the International Measurement Confederation**, 144: 234–242, (2019).

[40] Wang X., Xu S., Zhou S., Xu W., Leary M., Choong P., Qian M., Brandt M., and Xie Y. M., "Topological design and additive manufacturing of porous metals for bone scaffolds and orthopaedic implants: A review", **Biomaterials**, 83: 127–141, (2016).

[41] Wang D., Wu S., Fu F., Mai S., Yang Y., Liu Y., and Song C., "Mechanisms and characteristics of spatter generation in SLM processing and its effect on the properties", **Materials and Design**, 137: 33–37, (2018).